

Successful Reduction of Neointimal Hyperplasia on Stainless Steel Coronary Stents by Titania Nanotexturing

Aleena Mary Cherian, John Joseph, Manitha B. Nair, Shantikumar V. Nair, Vijayakumar Maniyal,* and Deepthy Menon*



Cite This: *ACS Omega* 2020, 5, 17582–17591



Read Online

ACCESS |



Metrics & More

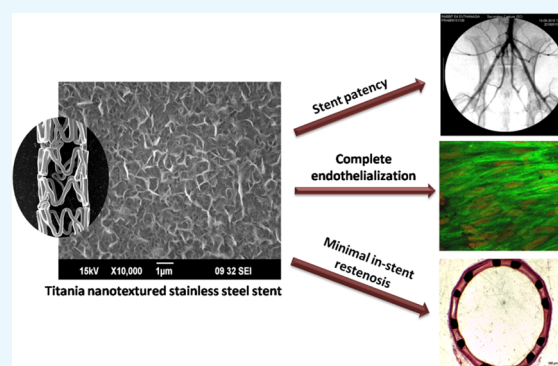


Article Recommendations



Supporting Information

ABSTRACT: Bare metal stents (BMSs) of stainless steel (SS) were surface engineered to develop nanoscale titania topography using a combination of physical vapor deposition and thermochemical processing. The nanoleafy architecture formed on the stent surface remained stable and adherent upon repeated crimping and expansion, as well as under flow. This titania nanoengineered stent showed a preferential proliferation of endothelial cells over smooth muscle cells in vitro, which is an essential requirement for improving the in vivo endothelialization, with concurrent reduction of intimal hyperplasia. The efficacy of this surface-modified stent was assessed after implantation in rabbit iliac arteries for 8 weeks. Significant reduction in neointimal thickening and thereby in-stent restenosis with complete endothelial coverage was observed for the nanotextured stents, compared to BMSs, even without the use of any antiproliferative agents or polymers as in drug-eluting stents. Nanotexturing of stents did not induce any inflammatory response, akin to BMSs. This study thus indicates the effectiveness of a facile titania nanotopography on SS stents for coronary applications and the possibility of bringing this low-priced material back to clinics.



1. INTRODUCTION

Drug-eluting stents have to a large extent reduced restenosis rates compared to bare metal stents (BMSs) and hence are the preferred choice currently in the clinics for the treatment of coronary artery diseases.¹ However, concerns remain around delayed healing, prolonged thrombosis risk,^{2,3} and long-term endothelial dysfunction, resulting in neoatherosclerosis in arteries implanted with drug-eluting stents (DESs).^{4–7} Thus, there is still a requirement to develop stents that retain the low restenosis rates of the current DESs and concurrently not compromise re-endothelialization.

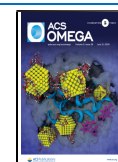
Stainless steel (SS) stents have been the material of choice for coronary stenting for several decades. However, the high restenosis rates preclude the use of bare metallic SS stents in the clinics. Several researchers have investigated surface modification strategies as a convenient method to improve re-endothelialization and thereby reduce in-stent restenosis. One such surface modification strategy exploited the benefits of biocompatible titanium nitride oxide surface coating (TiNOx) on SS stents. These stents (TITAN) showed a significant reduction in neointimal hyperplasia in comparison to bare SS in porcine model⁸ and in clinical trials.^{9–11} Additionally, topographical modifications at the nanoscale,^{12–14} including studies from our own group, have demonstrated the success of surface-modified SS¹⁵ and titanium (Ti)^{16,17} substrates in promoting endothelial cell

proliferation. Research has shown that titanium surfaces having submicron patterns with lateral dimensions >100 nm could efficiently promote endothelial cell adhesion,¹⁸ whereas titanium dioxide (TiO₂) nanostructures displayed a concomitant reduction in smooth muscle cell (SMC) proliferation with good endothelialization in vitro.^{19,20} The highest endothelial cell attachment with an intact endothelial cell layer under flow conditions and fastest migration of endothelial cells (ECs) was seen on nanometer to submicron features than flat surfaces. Significantly less platelet adhesion and improved endothelial responses were observed on nanometer rough titanium compared to flat counterparts, indicating the potential of these surface features in nanometer regime on titanium for vascular stent applications.²¹ Nanotopography was shown to provide nanoscale cues that facilitated cell sensing, migration, and probing, with more organized actin cytoskeletal filaments and locomotive features, which was not observed on a flat substrate of titanium.²² It has also been demonstrated that TiO₂ nanotubes represent a promising platform for stent as it

Received: May 3, 2020

Accepted: June 22, 2020

Published: July 7, 2020



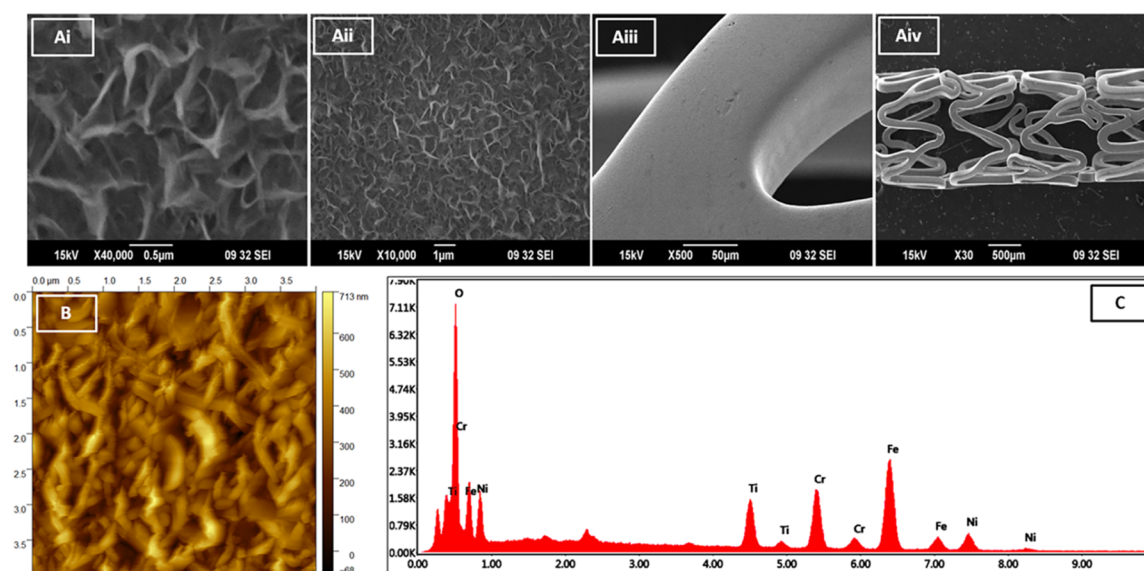


Figure 1. (A) SEM images of the nanotextured SS TNL stent at different magnifications showing uniformity in nanotexturing over the entire surface. (B) AFM images confirming the nanoleafy architecture on SS TNL. (C) EDAX measurements demonstrating the presence of titanium and oxygen on SS TNL.

could selectively regulate EC growth and SMC inhibition.^{19,23} Our group has also demonstrated in-depth studies on various titania nanostructures developed by hydrothermal processing on Ti substrates and the impact of nanoarchitecture in regulating cell response, blood compatibility, and so forth.^{16,17} All nanostructured surfaces showed significantly enhanced cellular viability and proliferation of ECs and substantially reduced SMC proliferation and platelet adhesion in comparison to unmodified titanium substrates.¹⁷ However, all these works are confined to in vitro studies, and only a few have been taken further for in vivo implantation. One such in vivo study was the development of titania nanotubular structures on metallic Ti stents that showed reduced restenosis (by ~30%) in comparison to bare Ti stents²⁴ and promoted faster functional endothelialization. Nevertheless, this technology cannot be translated to clinical use on BMSs as Ti is not a stent material. Moreover, an inflammatory response that would ordinarily result from exposure to bare metal SS stent was observed to be significantly reduced upon nanotexturing because of the masking of the underlying metallic ions by an oxide or nitride-rich surface layer.²⁵

Hence, with the aim of bringing an old horse back to the race, we explore the potential of SS stents having a titania surface nanotopography for reduced in-stent restenosis, as a sequel to the in vitro work that reported beneficial effects of this nanotexturing. This material displayed improved mechanical properties and corrosion resistance, with minimal metal-ion leaching from the surface.¹⁵ An interesting observation was the preferential adhesion and proliferation of ECs over SMCs in vitro.¹⁵ Herein, we extend this evaluation in vivo to prove that nanotexturing of BMSs without the use of any polymers or drugs helps to evade the problem of in-stent restenosis which is routinely observed in BMSs. How effective is the nanotextured titania layer on SS stents in promoting endothelialization is investigated after implantation of the stents in a rabbit iliac artery for 8 weeks, in comparison to BMSs.

2. RESULTS AND DISCUSSION

2.1. Nanosurface Modification and Characterization.

In the present study, titania nanotexturing was obtained on commercial bare metal SS stents after sputter depositing TiO₂ and its subsequent hydrothermal treatment as reported earlier.¹⁵ A distinctive uniform titania nanotopography [called hereafter as titania nanoleaf (TNL)] was generated on the abluminal and luminal surfaces of the SS stent (SS TNL), as can be noted from the scanning electron microscopy (SEM) images at different magnifications [Figures 1A(i–iv) and S1]. Individual nanoleaves having average dimensions of 115 ± 20 nm (thickness) and 650 ± 30 nm (length) were seen in the atomic force microscopy (AFM) images as well (Figure 1B). The sputtering current and time were optimized at 1 A for 20 min with an oxygen flow at 80 sccm after various trials to obtain a uniform nanotexturing on the stent surface that was mechanically stable without peeling off. Lower sputtering currents 0.5, 0.7, and 0.85 A and time 10, 20, or 30 min did not generate distinct and uniform nanostructures on the titania-coated SS surfaces (Figure S2). This could be mainly because lower deposition duration and current would not be sufficient to generate a uniform coverage of TiO₂ on the stent surface, whereas higher sputtering currents and time resulted in peeling off of the nanotextured titania layer from the stent surface upon expansion (Figure S3). This could be attributed to the formation of thicker TiO₂ films after sputter deposition for longer durations. It is already established that titanium oxide coatings thicker than ~25 nm can be unstable and are prone to peeling off under crimping and expansion.²⁶ The thickness of the deposited titania layer after sputter coating in our study was analyzed by AFM and was ~30 nm (Figure S4). This thin titania layer would ensure intactness of the nanostructures on the stent surface after expansion. Roughness analysis using AFM showed that titania nanotexturing produced a nanorough surface having an average roughness of 99.3 ± 5.1 nm in comparison to the surface devoid of nanotexturing, but with titania deposition (9.96 ± 4.3 nm) (Figure S5). It was remarkable to note that upon titania nanotexturing, bare metal surfaces turned highly hydrophilic with a water contact angle of

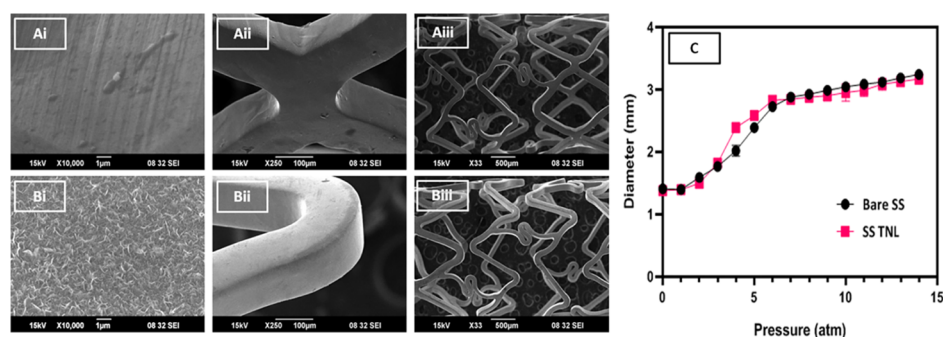


Figure 2. SEM images of (A) bare SS and (B) SS TNL stents at different magnifications after completion of 20 million cycles under flow. (C) Balloon expansion profiles of bare and nanotextured SS TNL stents.

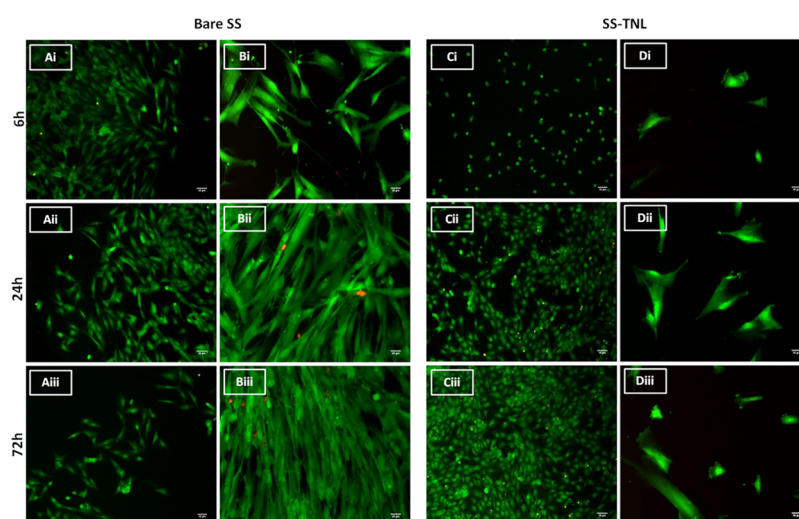


Figure 3. Live–dead fluorescence images of ECs seeded on (A) bare SS and (C) SS TNL stents at 6 [A(i),C(i)], 24 [A(ii),C(ii)], and 72 h [A(iii),C(iii)] and SMCs seeded on (B) bare SS and (D) SS TNL stents at 6 [B(i),D(i)], 24 [B(ii),D(ii)], and 72 h [B(iii),D(iii)].

$4.9 \pm 0.7^\circ$ in comparison to bare surface ($74.5 \pm 2.7^\circ$) (Figure S6). Surface compositional analysis of titania nanotextured SS stents carried out using XPS confirmed the formation of an oxide layer of TiO_2 in both the wide and high-resolution spectra (Figure S7). Although SS TNL had distinct peaks at 458.5 and 464.4 eV corresponding to the 4+ oxidation state of TiO_2 , this was totally absent in bare SS stents, proving that the stent has a titania-rich surface. Similar results were obtained on the samples when analyzed using energy-dispersive spectroscopy (EDAX) (Figure 1C), which reaffirmed the deposition of $\sim 8\%$ of titanium and 40% oxygen, signifying titanium dioxide formation in comparison to bare SS (Figure S8).

Stents being endovascular devices repeated crimping, and expansion is required for proper deployment. Moreover, it is important that the structures can withstand the shear stress because of continuous blood flow in the artery. Stent coating durability was studied under accelerated flow conditions in a simulated blood vessel to complete 20 million cycles, which is equivalent to 6 months of stent implantation in humans. As can be seen from the SEM images, there was no delamination or flaking of the nanotextures, indicating the mechanical stability of the coating [Figure 2B(i,iii)], with BMS as the control [Figure 2A(i–iii)]. No particulate matter could be retrieved from the circulating fluid at the end of the study duration when analyzed using SEM (data not shown), again pointing to the good adhesion of the nanostructures on the stent. The circulating fluid was also tested for any metallic ion

release using inductively coupled plasma mass spectroscopy (ICP–MS) analysis at different time points (2, 14, and 21 days). Results from ICP revealed the absence of any metallic ion content at all of the time points in PBS circulated through the nanotextured stent (data not shown). Nanotextured stents during their development are subjected to high temperature and pressure conditions in a hydrothermal chamber. To understand if this thermochemical treatment in any way altered its balloon expansion profiles, experiments were carried out in comparison to an unmodified bare SS stent. The graphs shown in Figure 2C clearly portray that the chemical processing of stents did not affect its expansion profile with increasing balloon expansion pressures. Moreover, regardless of the repeated crimping and expansion of stents during this experiment, the nanotextures remained adherent onto the stent surface as evident from SEM (Figure S9). All these results confirmed the usability of the nanotextured stent for in vivo implantation.

2.2. Cell Material Interaction Studies. In any physiological environment, protein adsorption always precedes cellular adhesion. Hence, to investigate the impact of nanotexturing on protein adsorption, analysis of total protein was carried out on the different substrates. Results shown in Figure S10 indicate that very fewer proteins ($< 5 \mu\text{g cm}^{-2}$) adhered onto SS TNL in comparison to the bare SS ($\sim 9 \mu\text{g cm}^{-2}$). This can be attributed to the super hydrophilic nature

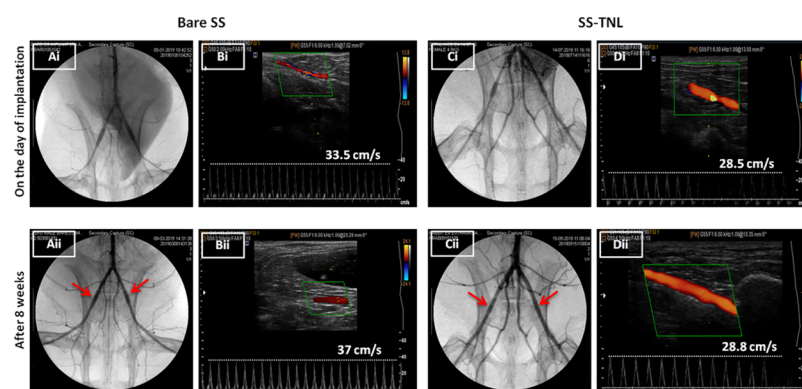


Figure 4. Angiogram and ultrasound images of bare [A(i),B(i)] and SS TNL [C(i),D(i)] stents on the day of implantation and after 8 weeks prior to euthanasia [A(ii),B(ii)] for bare; C(ii),D(ii) for SS TNL]. Arrows in the angiogram point to the stented site in the artery. The value for the blood flow velocity of the respective animal is depicted in the ultrasound panel.

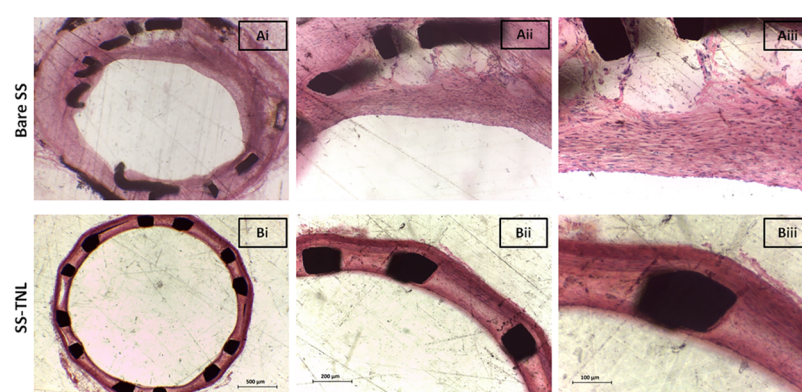


Figure 5. H&E images of (A) bare and (B) SS TNL stented vessels at 4 \times [A(i),B(i)], 10 \times [A(ii),B(ii)], and 20 \times [A(iii),B(iii)] magnifications.

of the nanotextured surface, which is known to influence protein adsorption in a significant way.²⁷

To understand the influence of the nanoscale architecture on vascular cell adhesion and proliferation, *in vitro* studies were carried out using human umbilical vein endothelial cells (HUVECs) and SMCs as a function of time. The results of live–dead staining done on the surfaces at early time periods (6 h) showed remarkable differences in the adhesion of HUVECs versus SMCs (Figure 3). It was seen that HUVECs at 6 h were dispersed evenly, with less spreading on the SS TNL substrate [Figure 3C(i)], perhaps owing to its superhydrophilicity, whereas cells on bare SS were clustered and found to be more spread [Figure 3A(i)]. These adhered cells on SS TNL showed significant proliferation with time, both quantitatively (Figure S11) and qualitatively [Figure 3C(ii,iii)], as against that of bare SS [Figure 3A(ii,iii)], correlating with our earlier results.¹⁵ These observations were in contrast to the results obtained using SMCs, wherein on SS TNL very few cells got adhered and proliferated from 6 to 72 h [Figure 3D(i–iii)], unlike those on bare substrates [Figure 3B(i–iii)]. These results clearly demonstrate the distinctive role of nanotopography in cellular adhesion and proliferation, with a preferential cell response.^{12,13} Such a preferential response is reported on titania surfaces having nanoscale topography (e.g., nanotubes).¹⁹

Additionally, complete endothelialization with stable cell-to-cell contacts, evident from the CD-31 staining, which is indicative of the formation of an integral endothelial monolayer, was apparent on the SS TNL surface (Figure

S12B), whereas on the bare surface this was lacking (Figure S12A). This endothelium was also found to be functional as expressed by its nitric oxide release as depicted in Figure S12C. This preferential response observed on nanorough versus smooth surfaces can be ascribed perhaps to the differences in the specific proteins that adsorb to the surfaces which favor ECs to SMCs. This aspect of the study is currently underway.

2.3. In Vivo Stent Implantation in Rabbit Iliac Arteries. To confirm if this extraordinary *in vitro* response of HUVECs versus SMCs will be replicated *in vivo*, SS TNL stents ($n = 8$) were implanted in rabbit iliac arteries for 8 weeks, with BMS as the control. No procedural deaths occurred, and all of the stents were successfully deployed and intact within the artery as manifested in the angiogram images taken on the day of implantation [Figure 4A(i),C(i)]. Stent patency and blood flow after 8 weeks of implantation were analyzed by angiogram and color Doppler images. There was no occlusion observed in any of the stent groups after 8 weeks of deployment, which confirmed stent patency [Figure 4A(ii),C(ii)]. This could also be established from the representative angiogram videos of both the study groups, after 8 weeks prior to euthanasia (Supporting Information Videos 1 and 2).

Blood flow velocities were also monitored using color Doppler before and after stent implantation [Figure 4B,D], clearly revealing no significant variations in the blood flow velocities. Moreover, post implantation Doppler data demonstrated no hindrances to the blood flow nor any thrombus occlusion in any of the stented arteries [Figure 4B(ii),D(ii)].

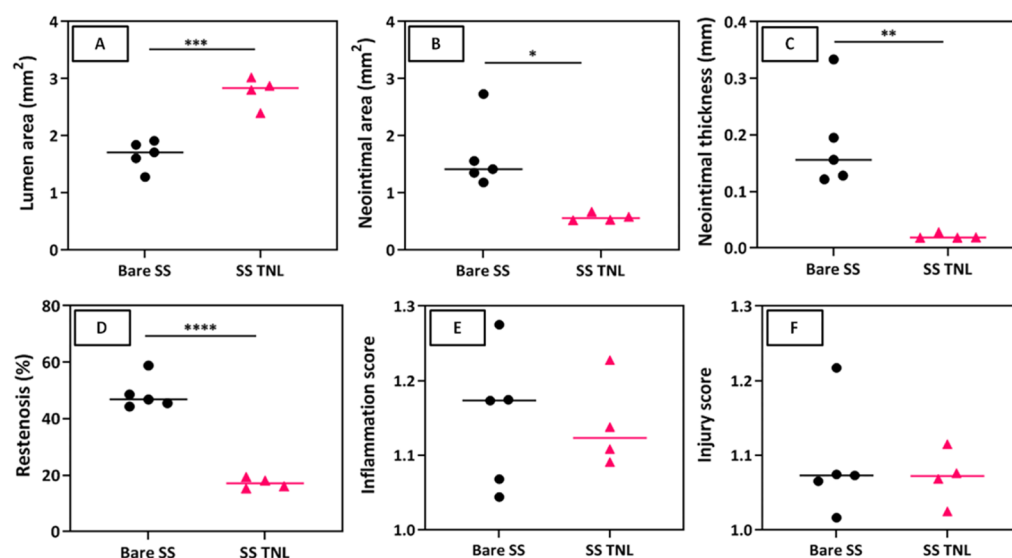


Figure 6. Histomorphometric analysis showing the (A) lumen area (mm^2), (B) neointimal area (mm^2), (C) neointimal thickness (mm), (D) restenosis (%), (E) inflammation score, and (F) injury score of the bare and nanotextured SS TNL stent-implanted vessel sections.

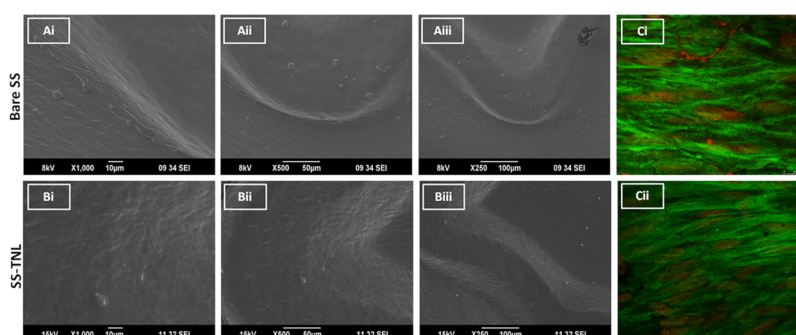


Figure 7. SEM images of [A(i–iii)] bare SS and [B(i–iii)] nanotextured SS TNL stent-implanted arteries at different magnifications and representative immunofluorescent *en face* stained images of wheat germ agglutinin on ECs in the [C(i)] bare and [C(ii)] SS TNL stented artery at a depth of $2 \mu\text{m}$ from the luminal surface (scale bar: $10 \mu\text{m}$).

Movies portraying the pulsatile blood flow through stented arteries are displayed in Supporting Information Videos 3 and 4.

2.4. Histology and Histomorphometric Analysis. One of the most exciting observations was evident from the histological analysis of stented arteries after 8 weeks of implantation. Significant lumen narrowing due to tissue ingrowth was noted in bare SS stent-implanted arteries [Figure 5A(i–iii)] and counter-to-minimal neointimal thickening was noted for SS TNL [Figure 5B(i–iii)]. Also, no in-stent thrombosis was seen in any of the stent groups. This implied that nanotextured SS stent (SS TNL) without the use of any drugs or polymers as in commercial DESs could inhibit the hyperproliferation of SMCs and thereby yielded minimal intimal thickening.

These results mean that the nanotexturing approach was able to reduce in-stent restenosis which is commonly observed upon implantation of BMSs. This marked difference in the qualitative results from H & E imaging is apparent from the quantitative histomorphometric measurements.

The lumen area for SS TNL was notably higher than that for bare SS, as can be seen from Figure 6A. A noteworthy decrease in neointimal thickness and neointimal area was noted in the arteries implanted with nanotextured SS TNL stents ($0.02 \pm 0.005 \text{ mm}$ and $0.58 \pm 0.07 \text{ mm}^2$) in comparison to bare (0.19

$\pm 0.9 \text{ mm}$ and $1.65 \pm 0.6 \text{ mm}^2$) stents (Figure 6B,C). On an average, nearly 50% decrease in neointimal stenosis (restenosis %) was observed in arteries with SS TNL stents ($17.24 \pm 1.85\%$) as against that of bare metal SS stents ($48.82 \pm 5.83\%$) (Figure 6D). These values correspond to an average of all of the stented sections from the proximal to the distal ends of the stented artery, wherein neointimal thickening was relatively high at the stent edges in comparison to the midpart of the stent as shown in Figure S13 for both bare and SS TNL stents.

The *in vivo* results obtained in our study indeed correlated well with the preferential vascular cell response observed *in vitro*, wherein the excessive hyper proliferation of SMCs is known to induce intimal thickening and thereby in-stent restenosis.²⁸ A plausible reason for this excellent *in vivo* result can be the inhibition of SMC proliferation coupled with the promotion of faster functional endothelium imparted by the nanotopography, very similar to the *in vitro* results. This apart, the nanotexturing approach on BMSs did not induce any inflammation or any injury at the stented site (Figure 6E,F). The major type of cells observed in the stented artery were neutrophils and lymphohistiocytes, in minimal numbers, implying the negligible inflammation induced by SS TNL.

2.5. Stent Strut Coverage and Endothelialization. To understand if the implanted stents had complete cell coverage at the end of 8 weeks, SEM and immunofluorescence staining

for ECs were carried out. It is widely reported in the literature that drug-eluting stents owing to the continuous elution of antiproliferative drugs lead to incomplete endothelialization, thereby exposing the stent struts.²⁹ To assess if nanotexturing would offer a different response, the luminal side of the explanted stents were imaged as shown in Figure 7A,B to see that all of the struts were totally covered with a cell-like layer for both bare and SS TNL. To reaffirm if this cell-like layer corresponds to an endothelium, an *en face* staining of the stent lumen was performed using an endothelium-specific FITC labeled wheat germ agglutinin (WGA), which stained the endothelial glycocalyx green, counter-stained with propidium iodide. Prior to this, a native blood vessel was stained with WGA vividly implying the specificity of this marker for ECs (Figure S14).

Representative confocal images of the stented artery at a depth of 2 μm from the surface of the lumen showed the presence of agglutinin-stained ECs, indicating a perfect endothelial coverage throughout the luminal surface over the stent struts in both bare and SS TNL groups [Figure 7C(i,ii)]. This could also be confirmed from the videos depicting the staining through the entire thickness of the stented vessel (Supporting Information Videos 5 and 6). BMSs are known to get endothelialized with total stent strut coverage within a duration of 4 weeks in rabbits,³⁰ supporting our results. The main highlight of our material is the good endothelialization together with minimal in-stent restenosis observed in vivo.

3. CONCLUSIONS

In this study, an innovative titania nanosurface engineering of SS bare metal coronary stents using a facile thermochemical processing technique provided a novel stent that exhibited remarkable in vivo performance when tested in rabbit iliac artery for 8 weeks. The features offered by this nanostent include (i) efficient endothelialization, (ii) minimal SMC adhesion, and (iii) no thrombus formation, thereby presenting a material endowed with minimal in-stent restenosis, a major complication otherwise encountered with BMSs. Notably, these characteristics are observed in the absence of any drug or polymer as in commercial DESs, which makes the material promising for a clinical translation.

4. EXPERIMENTAL SECTION

4.1. Surface Modification of Bare Metal Stainless Steel Stents. Nanoscale topographies were formed on bare metal SS stents (Crypton coronary stents, Meril Life Sciences, India) with length 8 mm and crimped diameter of 1.4 mm and medical grade 316L SS circular discs of 14 mm diameter procured from JayonSurgicals Pvt. Ltd., India. Silicon carbide abrasive papers with different grit sizes, diamond, and alumina suspensions (all procured from Buehler Inc. USA) were used to mechanically polish the SS discs. The polished discs were ultrasonically cleaned in acetone, ethanol, and distilled water and dried in air.

Stents and the polished discs were subjected to sputter coating by varying various parameters: (i) sputtering current (0.5, 0.7, 0.85, and 1 A), (ii) sputter duration (10, 20, and 30 min), and (iii) oxygen flow (50, 70, and 80 sccm) within a DC sputter coating unit (Cluster tool model-CT-150, Hind High Vacuum Pvt. Ltd, Bangalore, India). A sputtering current of 1 A for 20 min using pure Ti target with 80 sccm oxygen flow generated a homogeneously thin TiO_2 coating. In this

experiment, to confirm the development of a uniform coating, the stents were mounted onto a motor shaft rotated at a constant speed (6000 rpm) inside the sputtering chamber. Nanotexturing of SS stents/discs was carried out by a facile hydrothermal modification in 1 M sodium hydroxide solution at elevated temperature (200 $^\circ\text{C}$) for 4 h to produce a discrete nanomorphology as reported earlier by our own group.³¹ After hydrothermal treatment, the stents/discs were rinsed in distilled water for 10 min using an ultrasonic water bath and air-dried.

4.2. Surface Characterization of Nanotextured Surfaces. Surface nanotexturing on the luminal and abluminal areas of hydrothermally modified stents were examined using SEM (JEOL JSM-6490L, Japan). Additionally, the surface topography was analyzed by AFM (Agilent 5500 series). The dimensions of the nanoleaves were deduced from the AFM images using ImageJ software. Surface compositional analysis of the surfaces was investigated using energy-dispersive analysis (JOEL JSM-7610 fPlus) and X-ray photoelectron spectroscopy (XPS) (Axis Ultra DLD, Kratos Analyticals, UK) over a binding energy range of 0–1000 eV.

4.3. Durability and the Balloon Expansion Profile of Nanotextured Stents. Durability of the nanotexturing on SS stents was analyzed under flow in a simulated blood vessel with normal physiological conditions. The stents were expanded to its maximum diameter using a balloon catheter within a latex tubing (3 mm inner diameter) which was connected to a peristaltic pump (Masterflex L/S, Cole Palmer) with 600 rpm. Bare SS and SSTNL stents were deployed in two tubes with different reservoirs, and phosphate-buffered saline (ph 7.4) was circulated through the tubings. The reservoir was placed in a water bath at 37 $^\circ\text{C}$. The pump was set at 600 rpm, and the fluid was circulated for 22 days to complete 20 million cycles which is equivalent to 6 months of stent implantation in humans. The wall shear stress was calculated to be 1.5 Nm^{-2} from the Hagen Poiseuille equation. After completion of 22 days, in-flow stents were analyzed for the stability of nanostructures and the circulated fluid was visualized for any particulate matter using SEM. The circulated fluid was also aliquot at different time points 2, 7, and 22 days and checked for the metallic ion (Ti, Fe, Ni, and Cr) content using ICP-MS.

The balloon expansion profile of the nanotextured stents was studied in comparison to bare metal SS stents by using a pressure volume controller (GDS from USA). The stents were mounted onto a balloon catheter and was expanded to their maximum diameter by applying increasing pressures from 0 to 14 atm. After each expansion, the diameter of the stent was measured using a laser micrometer (Keyence LS3034), following which the same stent was crimped back onto the balloon and expanded further. This was done consecutively up to 14 atm. After the completion of the experiment, the stent was given for SEM analysis to visualize the stability of nanostructures on the stent surface after repeated crimping and expansion.

4.4. Cell Material Interaction Studies. HUVECs and human artery smooth muscle cells (HASMCs) were isolated from umbilical cord after informed patient consent. HUVECs were cultured in an EBM-2 (Lonza) endothelial cell basal medium with EGM-2 SingleQuots (Lonza) containing VEGF and HASMCs in SmBM (Lonza) SMC basal medium with SmGM-2 SingleQuots (Lonza) containing hFGF-B.

To study the viability of cells on nanotextured surfaces in comparison to the bare, HUVECs and HASMCs were seeded on both the substrates at a seeding density of 20,000 and 10,000 cells, respectively, for culture durations of 6, 24, and 72 h. After each time point, substrates with cells were taken out and washed in PBS once, following which the cells were stained with calcein, AM, and ethidium homodimer-1 live–dead viability/cytotoxicity staining kit (L3224, Invitrogen by Thermo Fisher Scientific) to visualize the live and dead cells on the substrates. HUVECs and HASMCs on both substrates were then viewed under a fluorescence microscope (Leica DMI3000 B, Leica Microsystems) and imaged. Alamar blue assay was carried out to assess cell proliferation on nanotextured SS in comparison to bare SS at 6, 24, and 72 h by seeding both the substrates with HUVECs and HASMCs at a seeding density of 16,000 cells cm^{-2} . At the end of each time point, cells were incubated with 10% Alamar blue (Invitrogen Bioservices Pvt. Ltd, Bangalore) in media for 4 h, and the optical density was recorded using a microplate reader (Synergy HI, Biotek) at 570 and 600 nm. The graphs were plotted as percentage cell viability with cells grown on control tissue culture plates normalized as 100%. To study the endothelialization potential, HUVECs were seeded on both the substrates at a seeding density of 16,000 cells cm^{-2} and incubated for 72 h in complete medium. After 3 days in culture, HUVECs cultured samples were washed and fixed using 4% paraformaldehyde in PBS. Cells were then blocked with 1% fetal bovine serum in PBS for 15 min followed by incubation with primary CD31/PECAM-1 antibody (JC/70A, Thermo Scientific) overnight at 4 °C. The cells were then stained with secondary Texas red conjugated anti-mouse secondary antibody (Thermo Scientific) for 1 h at room temperature (RT) followed by counter staining using DAPI and observed under a fluorescent microscope (Leica DMI3000 B, Leica Microsystems). To assess the functionality of ECs seeded on the substrates, nitric oxide (NO) release was estimated by modified Greiss assay. HUVECs were seeded on bare and SS TNL substrates at a seeding density of 16,000 cells cm^{-2} in complete EGM-2 media and cultured for 24 and 72 h. The culture medium was then isolated, and Greiss agent (Sigma-Aldrich, USA) was added to it and incubated for 15 min at RT. The NO released was quantified by optical density measurements at 540 nm, from the serially diluted sodium nitrate standard calibration curve.

4.5. In Vivo Stent Implantation in Rabbit Iliac Artery Model. In vivo stent implantation studies were done on New Zealand white rabbits (2.5–3 kg) after obtaining an approved ethical consent from the Institutional Animal Ethics Committee (Ref. no. IAEC/2015/3/8). A rabbit iliac artery model was used to investigate the effect of nanotextured SS stents in comparison to bare metal SS stents on in-stent restenosis post 8 weeks implantation. A total of eight rabbits ($n = 16$ stents) were stented, with four animals each receiving bare SS stents and nanotextured stents in both the iliac arteries. All of the animals were fed a regular diet and premedicated with aspirin (20 mg kg^{-1}) and clopidogrel (15 mg kg^{-1}) daily for 3 days prior to surgery. The anesthesia was administered with an intramuscular dose of xylazine (3 mg kg^{-1}), ketamine (50 mg kg^{-1}), and midazolam (0.3 mg kg^{-1}), and the condition was maintained using isoflurane throughout the surgery procedure. The vascular access was obtained after the left carotid artery was exposed through surgical cut-down. Carotid artery was mobilized in position using 3–0 silk sutures,

and the carotid artery was punctured using a 24G canula, followed by insertion of a 0.014" BMW guide wire under fluoroscopic guidance using a C-Arm (OEC 9800, GE Healthcare). A 4-Fr introducer sheath was advanced through the guide wire and held in position during the stenting procedure. The animal was heparinized (750 IU). Under fluoroscopic guidance by injecting contrast, the left and right iliac arteries were selected for stent deployment based on the targeted vessel diameter of 2–2.5 mm. Each stent was hand crimped on a 3.0 mm noncompliant angioplasty balloon and deployed (12 atm balloon inflation for 30 s) in the iliac artery of the rabbit to obtain an approximate balloon-to-artery ratio of 1.2:1. At the end of the procedure, a post deployment angiography was carried out. The arterial access site was then ligated using the silk sutures, and the incision was closed. The animals after recovery from anesthesia were moved to postoperative care. Eight weeks post stent deployment, animals underwent follow-up angiography to validate the patency of the arteries after stent placement. Animals were then euthanized, and stents were harvested and prepared for histopathology.

4.6. Ultrasound Imaging of Stented Arteries. Ultrasound images are taken using a color Doppler ultrasound (My Sono U6, Samsung health care) before the stenting procedure to obtain the iliac artery diameter and blood velocity. Post 8 weeks before the animals are sacrificed, ultrasound images of the stented arteries are taken. The site of stent implantation was located using an angiogram and marked following ultrasound imaging to obtain the blood flow velocity of the stented iliac arteries. The blood flow through the arteries and the blood velocity was recorded.

4.7. Histopathology and Histomorphometric Measurements. Histopathological evaluation of each implanted iliac artery was performed, after vessels surrounding the stents were isolated and embedded in methyl methacrylate and stained with hematoxylin–eosin (H&E). Histopathological sections were viewed under a microscope (Leica), and the measurements were taken using ImageJ software. Borders of lumen and internal elastic lamina were traced by hand, and the area circumscribed was calculated using the software. Lumen area, neointimal area, intimal thickness, and percentage stenosis were calculated from the H&E images. Internal elastic lamina area minus lumen area measured from the images denoted the morphometric measurement of neointimal area for the stented artery, and in-stent restenosis area was calculated as $[1 - (\text{lumen area}/\text{internal elastic lamina area})] \times 100$.

4.8. Evaluation of Arterial Injury. The arterial injury at the struts was determined based on the penetration of each strut into the vessel wall. Scores were assigned according to Schwartz et al.³² and were 0 when there was no injury, 1 for tear in the internal elastic lamina, 2 when struts perforated into the medial layer of the vessel, and 3 when the struts penetrated the external elastic membrane into the adventitia. Sum of individual injury scores was divided by the total number of struts in the section to obtain the average injury score.

4.9. Evaluation of Inflammation Scores. Inflammatory cells around the individual stent struts were observed under a microscope and graded. The sections were scored 0 for the absence of any kind of inflammatory cells surrounding the stent struts, 1 when light and very few inflammatory cells were present, 2 when moderate inflammation with more localized cellular aggregates were observed surrounding the struts, and 3

when dense lymphohistiocytic infiltration was present around the struts. Average of individual scores was divided by the total number of struts to obtain the total inflammation score for each stented section.³³

4.10. Stent Strut Coverage. The stent strut coverage was analyzed for all of the stented sections. The vessel sections were fixed in 10% neutral buffered formalin and cut open to expose the luminal side of the stent. The stented sections were then dehydrated in gradients of ethanol (50–100%) and dried. The dehydrated stented vessel sections were then gold-coated and imaged using SEM.

4.11. Endothelialization of the Stented Iliac Arteries. En face staining of stented iliac arteries was carried out using confocal microscopy (Leica TCS SP5II, Leica Microsystems). The tissue sections were cut open with the luminal side facing outward. The sections were washed with phosphate-buffered saline (PBS), followed by an antigen retrieval step in which sections are boiled in citrate buffer (pH ~ 6) on a water bath for 20 min. The sections were then rinsed twice in PBS following permeabilization using 0.5% triton and then incubation in 1% bovine serum albumin (BSA) for 1 h at room temperature. The samples were again rinsed with PBS and stained with 10 $\mu\text{g mL}^{-1}$ FITC Agglutinin (WGA, Vector labs) antibody for 1 h. The tissue samples are then counterstained with propidium iodide (Invitrogen, Thermo Fisher Scientific) nuclear stain for 10 min. Tissue samples are then incubated in Sudan black to eliminate autofluorescence followed by sandwiching between two confocal cover glasses.

4.12. Statistical Analysis. All of the measurements are denoted as mean \pm standard deviation. To compare between two groups, Student's *t*-test was used and analysis of variances (ANOVA) was done for multiple group comparisons. All of the statistical analyses were completed using graph pad prism software, and *p* values less than 0.05 were considered statistically significant.

■ ASSOCIATED CONTENT

SI Supporting Information

The Supporting Information is available free of charge at <https://pubs.acs.org/doi/10.1021/acsomega.0c02045>.

SEM images of nanotextured SS stents on the luminal surface (Figure S1); SEM images of TiO₂-coated stent surfaces at lower sputter current and time (Figure S2); SEM images of hydrothermally treated TiO₂-coated stent surfaces at higher sputter current and time after expansion (Figure S3); thickness of the sputter deposited titania layer evaluated from AFM (Figure S4); mean roughness analysis (Figure S5); water contact angle measurements (Figure S6); XPS analysis (Figure S7); EDAX measurements (Figure S8); SEM images of nanotextured stent after repeated crimping and expansion (Figure S9); amount of proteins adsorbed on the surfaces (Figure S10); endothelial and smooth muscle cell viability by alamar assay (Figure S11); CD31 staining of ECs and nitric oxide released from endothelial cell seeded substrates (Figure S12); H and E images showing neointimal thickening at the ends of the stented vessel (Figure S13); and normal rabbit blood vessel stained with endothelium-specific FITC-Agglutinin and propidium iodide nuclear stain (Figure S14) (PDF)

Angiogram video of bare stent-implanted rabbit iliac artery after 8 weeks of implantation and prior to euthanasia (AVI)

Angiogram video of SS TNL stent-implanted rabbit iliac artery after 8 weeks of implantation and prior to euthanasia (AVI)

Doppler ultrasound video portraying pulsatile blood flow of bare stent-implanted artery after 8 weeks of implantation (AVI)

Doppler ultrasound video portraying pulsatile blood flow of SS TNL stent-implanted artery after 8 weeks of implantation (AVI)

Confocal en face staining of WGA on endothelial cells in bare SS stented artery after 8 weeks of implantation. Depth of tissue scanned here is 5 μm (AVI)

Confocal en face staining of WGA on endothelial cells in SS TNL stented artery after 8 weeks of implantation. Depth of tissue scanned here is 5 μm (AVI)

■ AUTHOR INFORMATION

Corresponding Authors

Vijayakumar Maniyal – Department of Cardiology, Amrita Institute of Medical Science and Research Centre, Amrita Vishwa Vidyapeetham, Cochin 682041, Kerala, India; Email: drmvijay@aims.amrita.edu

Deepthy Menon – Amrita Centre for Nanosciences and Molecular Medicine, Amrita Vishwa Vidyapeetham, Cochin 682041, Kerala, India; orcid.org/0000-0003-2772-2276; Email: deepthymenon@aims.amrita.edu

Authors

Aleena Mary Cherian – Amrita Centre for Nanosciences and Molecular Medicine, Amrita Vishwa Vidyapeetham, Cochin 682041, Kerala, India

John Joseph – Amrita Centre for Nanosciences and Molecular Medicine, Amrita Vishwa Vidyapeetham, Cochin 682041, Kerala, India

Manitha B. Nair – Amrita Centre for Nanosciences and Molecular Medicine, Amrita Vishwa Vidyapeetham, Cochin 682041, Kerala, India; orcid.org/0000-0002-5567-6820

Shantikumar V. Nair – Amrita Centre for Nanosciences and Molecular Medicine, Amrita Vishwa Vidyapeetham, Cochin 682041, Kerala, India

Complete contact information is available at: <https://pubs.acs.org/doi/10.1021/acsomega.0c02045>

Notes

The authors declare no competing financial interest.

■ ACKNOWLEDGMENTS

The authors acknowledge the financial assistance provided by Department of Biotechnology, Government of India, through a project grant (no. BT/PR3516/Med/32/192/2011). One of the authors (Aleena) expresses her gratitude to Indian Council of Medical Research for her SRF Fellowship. The authors also acknowledge Dr. Dhamodaran for his help with sputter coating experiments, Sajin P Ravi for SEM and EDAX analyses, Department of Physics (CUSAT) for AFM measurements, Sarath. S for XPS analysis, and Dennis Mathew for confocal imaging. They also express gratitude to Dr. A. K. K. Unni and animal house staff for their help with animal experiments and

Amrita Vishwa Vidyapeetham for providing all infrastructural support for successful completion of the work.

■ ABBREVIATIONS

BMSs, bare metal stents; SS, stainless steel; DESs, drug-eluting stents; TiNO_x, titanium nitride oxide; Ti, titanium; TiO₂, titanium dioxide; ECs, endothelial cells; SMCs, smooth muscle cells; TNL, titania nanoleaf; SEM, scanning electron microscopy; AFM, atomic force microscopy; XPS, X-ray photoelectron spectroscopy; EDAX, energy-dispersive spectroscopy; ICP-MS, inductively coupled plasma mass spectroscopy; WGA, wheat germ agglutinin; PBS, phosphate-buffered saline

■ REFERENCES

- (1) Jensen, L. O.; Christiansen, E. H. Are drug-eluting stents safer than bare-metal stents? *Lancet* **2019**, *393*, 2472–2474.
- (2) Byrne, R. A.; Joner, M.; Kastrati, A. Stent thrombosis and restenosis: what have we learned and where are we going? The Andreas Grüntzig Lecture ESC 2014. *Eur. Heart J.* **2015**, *36*, 3320–3331.
- (3) Kerkmeijer, L. S.; Tenekecioglu, E.; Wykrzykowska, J. J. Stent thrombosis in patients with drug-eluting stents and bioresorbable vascular scaffolds. The feared complication. *Pol. Arch. Intern. Med.* **2018**, *128*, 943–950.
- (4) Cornelissen, A.; Vogt, F. J. The effects of stenting on coronary endothelium from a molecular biological view: Time for improvement? *J. Cell Mol. Med.* **2019**, *23*, 39–46.
- (5) van den Heuvel, M.; Sorop, O.; van Beusekom, H. M.; van der Giessen, W. J. Endothelial dysfunction after drug eluting stent implantation. *Minerva Cardioangiol.* **2009**, *57*, 629–43.
- (6) Uchicado, Y.; Yoshino, S.; Takumi, T.; Kanda, D.; Ohmure, K.; Tabata, H.; Anzaki, K.; Ohishi, M. P1695 Impaired endothelial function is associated with neointimal abnormalities after drug-eluting stents deployment assessed by optical coherence tomography in patients with ischemic heart disease. *Eur. Heart J.* **2018**, *39*, No. ehy565.
- (7) Kern, M. J. Persistent endothelial dysfunction after drug-eluting stents: another continuing cost of reducing restenosis. *JACC Cardiovasc. Interv.* **2008**, *1*, 72–73.
- (8) Windecker, S.; Mayer, I.; De Pasquale, G.; Maier, W.; Dirsch, O.; De Groot, P.; Wu, Y.-P.; Noll, G.; Leskosek, B.; Meier, B.; Hess, O. M. Stent coating with titanium-nitride-oxide for reduction of neointimal hyperplasia. *Circulation* **2001**, *104*, 928–933.
- (9) Windecker, S.; Simon, R.; Lins, M.; Klauss, V.; Eberli, F. R.; Roffi, M.; Pedrazzini, G.; Moccetti, T.; Wenaweser, P.; Togni, M.; Tüller, D.; Zbinden, R.; Seiler, C.; Mehilli, J.; Kastrati, A.; Meier, B.; Hess, O. M. Randomized Comparison of a Titanium-Nitride-Oxide-Coated Stent With a Stainless Steel Stent for Coronary Revascularization. *Circulation* **2005**, *111*, 2617–2622.
- (10) Tuomainen, P. O.; Ylitalo, A.; Niemelä, M.; Kervinen, K.; Pietilä, M.; Sia, J.; Nyman, K.; Nammas, W.; Airaksinen, K. E. J.; Karjalainen, P. P. Five-year clinical outcome of titanium-nitride-oxide-coated bioactive stents versus paclitaxel-eluting stents in patients with acute myocardial infarction: Long-term follow-up from the TITAX AMI trial. *Int. J. Cardiol.* **2013**, *168*, 1214–1219.
- (11) Karjalainen, P. P.; Niemelä, M.; Airaksinen, J. K. E.; Rivero-Crespo, F.; Romppanen, H.; Sia, J.; Lalmand, J.; de Bruyne, B.; Debelder, A.; Carlier, M.; Nammas, W.; Ylitalo, A.; Hess, O. M. A prospective randomised comparison of titanium-nitride-oxide-coated bioactive stents with everolimus-eluting stents in acute coronary syndrome: the BASE-ACS trial. *EuroIntervention* **2012**, *8*, 306–315.
- (12) Bedair, T. M.; ElNaggar, M. A.; Joung, Y. K.; Han, D. K. Recent advances to accelerate re-endothelialization for vascular stents. *J. Tissue Eng.* **2017**, *8*, 2041731417731546.
- (13) Tan, C. H.; Muhamad, N.; Abdullah, M. M. A. B. Surface Topographical Modification of Coronary Stent: A Review. *IOP Conf. Ser.: Mater. Sci. Eng.* **2017**, *209*, 012031.
- (14) Loya, M. C.; Brammer, K. S.; Choi, C.; Chen, L.-H.; Jin, S. Plasma-induced nanopillars on bare metal coronary stent surface for enhanced endothelialisation. *Acta Biomater.* **2010**, *6*, 4589–4595.
- (15) Mohan, C. C.; Cherian, A. M.; Kurup, S.; Joseph, J.; Nair, M. B.; Vijayakumar, M.; Nair, S. V.; Menon, D. Stable titania nanostructures on stainless steel coronary stent surface for enhanced corrosion resistance and endothelialization. *Adv. Healthcare Mater.* **2017**, *6*, 1601353.
- (16) Mohan, C. C.; Chennazhi, K. P.; Menon, D. In vitro hemocompatibility and vascular endothelial cell functionality on titania nanostructures under static and dynamic conditions for improved coronary stenting applications. *Acta Biomater.* **2013**, *9*, 9568–9577.
- (17) Mohan, C. C.; Sreerexha, P. R.; Divyarani, V. V.; Nair, S.; Chennazhi, K.; Menon, D. Influence of titania nanotopography on human vascular cell functionality and its proliferation in vitro. *J. Mater. Chem.* **2012**, *22*, 1326–1340.
- (18) Lu, J.; Khang, D.; Webster, T. J. Greater endothelial cell responses on submicron and nanometer rough titanium surfaces. *J. Biomed. Mater. Res., Part A* **2010**, *94A*, 1042–1049.
- (19) Peng, L.; Eltgroth, M. L.; LaTempa, T. J.; Grimes, C. A.; Desai, T. A. The effect of TiO₂ nanotubes on endothelial function and smooth muscle proliferation. *Biomaterials* **2009**, *30*, 1268–1272.
- (20) Choudhary, S.; Haberstroh, K. M.; Webster, T. J. Enhanced functions of vascular cells on nanostructured Ti for improved stent applications. *Tissue Eng.* **2007**, *13*, 1421–1430.
- (21) Lu, J.; Yao, C.; Yang, L.; Webster, T. J. Decreased Platelet Adhesion and Enhanced Endothelial Cell Functions on Nano and Submicron-Rough Titanium Stents. *Tissue Eng. A* **2012**, *18*, 1389–1398.
- (22) Brammer, K. S.; Oh, S.; Gallagher, J. O.; Jin, S. Enhanced cellular mobility guided by TiO₂ nanotube surfaces. *Nano Lett.* **2008**, *8*, 786–793.
- (23) Peng, L.; Barczak, A. J.; Barbeau, R. A.; Xiao, Y.; LaTempa, T. J.; Grimes, C. A.; Desai, T. A. Whole genome expression analysis reveals differential effects of TiO₂ nanotubes on vascular cells. *Nano Lett.* **2010**, *10*, 143–148.
- (24) Nuhn, H.; Blanco, C. E.; Desai, T. A. Nanoengineered Stent Surface to Reduce In-Stent Restenosis in Vivo. *ACS Appl. Mater. Interfaces* **2017**, *9*, 19677–19686.
- (25) Bassous, N.; Cooke, J. P.; Webster, T. J. Enhancing Stent Effectiveness with Nanofeatures. *Methodist Debakey Cardiovasc J.* **2016**, *12*, 163–168.
- (26) Leng, Y. X.; Wang, J.; Yang, P.; Chen, J. Y.; Huang, N. The adhesion and clinical application of titanium oxide film on a 316 L vascular stent. *Surf. Coat. Technol.* **2019**, *363*, 430–435.
- (27) Stallard, C. P.; McDonnell, K. A.; Onayemi, O. D.; O’Gara, J. P.; Dowling, D. P. Evaluation of protein adsorption on atmospheric plasma deposited coatings exhibiting superhydrophilic to superhydrophobic properties. *Biointerphases* **2012**, *7*, 31.
- (28) Marx, S. O.; Totary-Jain, H.; Marks, A. R. Vascular Smooth Muscle Cell Proliferation in Restenosis. *Circ.: Cardiovasc. Interventions* **2011**, *4*, 104–111.
- (29) Arbustini, E.; Favalli, V.; Narula, J. Functionally Incomplete Re-Endothelialization of Stents and Neoatherosclerosis. *JACC Cardiovasc. Interv.* **2017**, *10*, 2388–2391.
- (30) Koppa, T.; Cheng, Q.; Yahagi, K.; Mori, H.; Sanchez, O. D.; Feygin, J.; Wittchow, E.; Kolodgie, F. D.; Virmani, R.; Joner, M. Thrombogenicity and early vascular healing response in metallic biodegradable polymer-based and fully bioabsorbable drug-eluting stents. *Circ.: Cardiovasc. Interventions* **2015**, *8*, No. e002427.
- (31) Divya Rani, V. V.; Manzoor, K.; Menon, D.; Selvamurugan, N.; Nair, S. V. The design of novel nanostructures on titanium by solution chemistry for an improved osteoblast response. *Nanotechnology* **2009**, *20*, 19S101.

(32) Schwartz, R. S.; Huber, K. C.; Murphy, J. G.; Edwards, W. D.; Camrud, A. R.; Vlietstra, R. E.; Holmes, D. R. Restenosis and the proportional neointimal response to coronary artery injury: Results in a porcine model. *J. Am. Coll. Cardiol.* **1992**, *19*, 267–274.

(33) Schwartz, R. S.; Edelman, E.; Virmani, R.; Carter, A.; Granada, J. F.; Kaluza, G. L.; Chronos, N. A. F.; Robinson, K. A.; Waksman, R.; Weinberger, J.; Wilson, G. J.; Wilensky, R. L. Drug-eluting stents in preclinical studies: updated consensus recommendations for pre-clinical evaluation. *Circ.: Cardiovasc. Interventions* **2008**, *1*, 143–153.